Research Square

Preprints are preliminary reports that have not undergone peer review.
They should not be considered conclusive, used to inform clinical practice,
or referenced by the media as validated information.

Green Tea-mediated Nanohydroxyapatite-reinforced Alginate composite scaffold for sequential dual-drug delivery for dental bone regeneration

Ananya N Nayak
Ramaiah Institute of Technology
Roshni Ramachandran
roshniramu@msrit.edu

Ramaiah Institute of Technology
Hansel P. Shah
Ramaiah Institute of Technology
Ishani Chowdhary
Ramaiah Institute of Technology
Punya Sharma
Ramaiah Institute of Technology

Research Article

Keywords: Dental tissue engineering, Nanocomposites, Nanohydroxyapatite, Osteogenesis, Scaffold

Posted Date: October 22nd, 2026

DOI: https://doi.org/10.21203/rs.3.rs-11263851/v1

License: This work is licensed under a Creative Commons Attribution 4.0 International License. Read Full License

Additional Declarations: No competing interests reported.

Abstract

Traumatic dental injury is frequently complicated by infection, inflammation, and bone loss, highlighting the need for dual drug delivery scaffolds that address these challenges simultaneously. This study developed and evaluated a green tea-mediated nanohydroxyapatite-integrated alginate nanocomposite scaffold with sequential dual-drug delivery. Green tea-mediated nanohydroxyapatite(nHAp) was synthesized, capped with amoxicillin, and integrated into an alginate matrix; the surface was coated with paracetamol to achieve rapid release of the analgesic and prolonged release of the antibiotic. X-ray diffraction, Fourier transform infrared spectroscopy, and scanning electron microscopy validated nHAp synthesis, drug integration and an interconnected scaffold morphology. Compared to pure alginate, the composite scaffold showed ▯370.49 percentage points higher swelling (Day 11) and a slowed degradation rate by ▯46.81 percentage points(Day 15), with rapid release of paracetamol and prolonged release of amoxicillin. The scaffold showed excellent cytocompatibility (> 92% viability across three cell types),a progressive increase in alkaline phosphatase activity over 21 days, and apatite formation in simulated body fluid, indicating in vitro osteogenic potential. Leachates of the amoxicillin-loaded scaffold produced larger zones of inhibition against Escherichia coli than free amoxicillin on days 1 to 6 Unlike previous studies on Nanohydroxyapatite(nHAp)-alginate composites that target only osteogenesis or provide only a single sustained-release profile, this scaffold combines green synthesis, mineral reinforcement by nHAp, and phase-specific dual drug delivery in a single platform; these in vitro findings support its further evaluation for dental bone tissue engineering.

1) Introduction

Biopolymer-based nanocomposite scaffolds have emerged as a key player in tissue engineering, where the polymer matrix influences swelling, degradation, integration, and release of the bioactive agents. Among the materials used in scaffold fabrication, alginate composites integrated with an inorganic mineral phase are in high demand for hard tissue regeneration, such as in the case of traumatic dental injury. Traumatic dental injuries affect a significant proportion of the world population, often resulting in enamel fractures and concussion to complete tooth avulsion[1–4]. Severe traumatic injuries are frequently associated with alveolar bone loss, leading to a considerable regenerative challenge. Besides structural damage, these injuries lead to an acute inflammatory response and infection of pulp and periapical tissues. Consequently, inflammation, infection, and bone loss occur simultaneously and collectively compromise the regenerative process [5]. Efficient clinical management requires a treatment strategy capable of addressing these challenges simultaneously, as unresolved inflammation and infection hinder bone healing [4].

In cases of severe traumatic dental injuries, traditional dental implants are used to replace the missing teeth. However, the procedure to fit dental implants is invasive and does not regenerate the alveolar bone, periodontal ligament, blood vessels, or nerves, resulting in limited restoration of natural tissue function. The success rate also depends on sufficient bone volume, often requiring additional grafting procedures in cases of traumatic bone loss [6]. These disadvantages leave a therapeutic timeframe in which regeneration of the native bone architecture, as an alternative to its mechanical replacement, would enhance the management of the underlying tissue deficit.

Dental bone tissue engineering addresses these limitations by utilizing scaffolds, growth factors, and cell-based approaches for bone regeneration rather than just substituting it [7–8]. Scaffold-based approaches

specifically support vascular ingrowth and biological integration with native tissue while allowing the physical design to be adapted to the geometry of the site of defect, customizing them to the irregular bone patterns seen post-trauma [9]. The performance of the scaffolds largely depends on the choice of constituent polymer-mineral system, which in turn influences biocompatibility, degradation behaviour, and osteogenic properties [10–15].

Alginate is commonly used in this context because its gelation property and degradation profile can be tailored to match the demands of alveolar bone regeneration while upholding an osteogenic microenvironment [16]. Integrating hydroxyapatite further enhances the performance of the scaffold by replicating the mineral phase of bone, which promotes osteogenesis and biocompatibility [17]. Alginate was selected over other natural polymers (e.g., chitosan, collagen, gelatin) due to its mild, room-temperature ionic gelation with Ca^{2+} and its avoidance of harsh crosslinkers; its porosity and degradation are tunable, and its carboxylate-rich backbone offers binding sites for nHAp and drug molecules while retaining an osteogenic, hydrated microenvironment. Green tea extract was chosen for the green synthesis due to its high polyphenol(catechin/EGCG) content, which acts as a capping and reducing agent and offers intrinsic antioxidant and antibacterial activity, which is beneficial at an infection-prone dental defect site. Nanohydroxyapatite synthesized utilising phytochemicals as capping agents, like green tea extract, provides additional benefits in comparison to conventional synthesis processes by enhancing the antimicrobial activity and biocompatibility, making the scaffold suitable for dental tissue engineering applications [18, 19].

Besides these advances, most alginate-based composite scaffolds from previous studies have been primarily focused on enhancing bone regeneration [7, 11, 16], with comparatively less emphasis on simultaneous management of pain and infection that is critical to traumatic dental injuries. Although drug-loaded scaffold systems have been extensively researched, they are specifically designed to offer a sustained or continuous release profile rather than one that provides for the dynamic biological demands of wound healing [15]. Amoxicillin and paracetamol were chosen for this study as they are the first-line, widely prescribed therapeutics in dental practice for treating post-traumatic dental injury infection and inflammation, and their different physicochemical profiles complement different release compartments (surface-coated painkiller vs. nHAp-capped antibiotic). For traumatic dental injury, efficient treatment requires rapid analgesic delivery during the early inflammatory stage, followed by prolonged antibacterial protection during the bone regeneration period, as the healing tissue remains susceptible to microbial infection [5]. A sequential release is therefore more advantageous than simultaneous release, as pain peaks within hours and needs rapid relief, whereas infection risk prevails for days to weeks, so syncing each drug's kinetics to its clinical window avoids both under-treatment during the early pain and premature exhaustion of the antibiotic. Scaffold systems capable of incorporating osteogenic support with a sequential drug release strategy remain relatively unexplored for alveolar bone regeneration post-traumatic dental injury[15–20].

To bridge this gap, the present study developed a green tea-mediated nanohydroxyapatite-reinforced alginate composite scaffold as a multifunctional platform that combines mineral reinforcement with compartmentalised, sequential drug delivery. Integrating paracetamol and amoxicillin as a dual drug delivery system, designed for rapid release of paracetamol for immediate pain relief, followed by prolonged release of amoxicillin for extended protection from infection during bone regeneration. We hypothesized that integrating sequential dual drug delivery with an osteogenic nanocomposite scaffold would offer rapid analgesic

availability and prolonged antibacterial activity while supporting osteogenic cell function in vitro, as a first step towards alveolar bone regeneration after traumatic dental injury.

2) Materials and methods

2.1) Materials and chemicals.

Ammonium dihydrogen orthophosphate was procured from Karnataka Fine Chem; sodium alginate was procured from SRL Chemicals Ltd; calcium chloride was procured from SDFCL Ltd, Mumbai. Tetley Green Tea Long Leaf Original was used for the extract preparation.

2.2) Nanohydroxyapatite (nHAp) synthesis.

2.2.1) Extract preparation

Green tea Leaves were finely ground into powder form using a mixer.10 mg of this leaf powder was added to 50 mL of deionized water & boiled for 2 hours. Once cooled, the mixture was filtered using Whatman filter paper, and the extract obtained was stored at 4ºC for further experiments.

2.2.2) Green synthesis of nHAp.

10 mL of 0.1 M calcium chloride was added to 10 mL of 0.6 M ammonium dihydrogen orthophosphate solution and mixed using a magnetic stirrer to form a homogeneous mixture. This was followed by adjusting the pH to 12 using 0.8 M NaOH, after which the mixture was added with 5 mL of the green tea leaf extract was added to the mixture and mixed using a magnetic stirrer for 1 hour, and left undisturbed at room temperature to get a gelatinous precipitate. The obtained gelatinous precipitate was dried in a microwave oven for 10 minutes and then dried in a 100ºC furnace for 1 hour. The dried cake was crushed to derive nanohydroxyapatite [21].

2.2.3) Characterization of nHAp.

The synthesised nHAp was characterised by X-ray diffraction to confirm its molecular composition and crystalline phase. The nHAp was tested at room temperature using a Panalytical diffractometer (Xpert Pro powder). (Cu Kα radiation) working at a voltage of 40 kV. X-ray diffraction (XRD) was carried out at a 2θ angle range of 10–70º, and the process parameters were kept as: scan step time 0.05 s and scan step size 0.02º [22, 23].

2.3) Preparation of scaffold integrated with nHAp.

2.3.1) Optimization of the alginate concentrations.

4%, 6%, and 8% sodium alginate solutions were prepared. They were individually mixed with 10 mg of nanohydroxyapatite and poured into separate Petri plates. They were polymerised by adding $CaCl_2$ solution dropwise with constant stirring to ensure uniform solidification. The samples were kept in the freezer for 24 hours and then subjected to lyophilisation.

2.3.2) Preparation of nHAp-embedded alginate scaffold.

After optimisation, 8% alginate was chosen for further experiments as it showed the most promising in vitro properties. For scaffold preparation, an 8% alginate solution was used, and 10 mg of nHAp was added to it and subjected to continuous stirring using a magnetic stirrer. This mixture was then treated with chilled $CaCl_2$ for crosslinking [24]. After 15 minutes of incubation at room temperature, the sample was lyophilised to obtain scaffolds of the same.

2.4) Characterization of Scaffold.

2.4.1) XRD analysis

The scaffolds fabricated were subjected to XRD analysis. The structure of the composite scaffold was analysed with the help of XRD studies. XRD patterns of the composite scaffolds were evaluated under standard conditions using a Panalytical diffractometer (XPERT Pro powder). (Cu K radiation) operating at a voltage of 40 kV. XRD was carried out for the 2-theta angle range of 10–70º, and the process parameters were kept as follows: 0.05 s for the scan step time and 0.02º for the scan step size [25].

2.4.2) SEM analysis

The nHAp-integrated alginate scaffold was cut into small pieces and subjected to gold sputtering for two minutes using a DII-29030SCTRSmart coater, followed by SEM-EDS analysis using Ultra55 FE-SEM Carl Zeiss EDS [26, 27].

2.4.3) Swelling analysis:

The 8% alginate scaffold without the integration of nHAp was taken as the control sample, and the scaffold with the integration of nHAp was taken as the Test sample. The dry weights of the scaffolds were noted. Scaffolds were then placed into the prepared phosphate-buffered saline (PBS) solution separately. The wet-weight scaffolds were weighed for 15 days (Day 1,3,5,9,11,15), and a graph of swelling % was plotted against time [28, 29]. The swelling percentage was calculated using Eq. 1. The experiment was carried out in triplicate.

$$\text{Swelling\%} = ((W_t - W_o)/W_o) * 100 \quad -(1)$$

Wherein W_t is the wet weight of the scaffold at time t, and W_o is the initial dry weight of the scaffold on day 0.

2.4.4) Degradation studies:

The 8% alginate scaffold without the integration of nHAp was taken as the control sample, and the scaffold with the integration of nHAp was taken as the test sample. The dry weights of the scaffolds were taken before the experiment. The pre-weighed scaffolds were added to the PBS buffer solution with lysozyme. The scaffolds were weighed at Days 5,7,9,11, and 15. A weight v/s day graph was plotted for the degradation ratio values [30]. The degradation percentage was calculated using Eq. 2. The experiment was carried out in triplicate.

$$\text{Degradation percentage} = ((W_o - W_t)/W_o) * 100 \quad -(2)$$

Wherein W_t is the wet weight of the swollen scaffold at time t, and W_o is the initial weight of the dry scaffold on Day 0.

2.5) Drug loading and release studies

2.5.1) Preparation of a standard curve for antibiotic and painkiller:

Standard graphs of the chosen antibiotic (Amoxicillin) and painkiller (Paracetamol) were individually plotted for concentrations 0.05,0.1,0.25,0.5,1,1.5 mg/mL at 270 and 196 nm, respectively.

2.5.2) Capping of Antibiotic to nHAp:

An optimised concentration of Amoxicillin solution was prepared and used for capping Amoxicillin onto nHAp in amoxicillin :nHAp ratios (w/w) of 1:1 and 1:2. The amoxicillin-capped nHAp was dried, integrated into the alginate scaffolds individually, and subjected to lyophilization.

2.5.3) Antibiotic (Amoxicillin) release profile studies

For evaluating the release profile of antibiotics, the antibiotic-capped nHAp-embedded alginate scaffold was immersed in PBS solution, and spectrometric analysis of the solution was carried out at 270 nm for specific time intervals of 15 to 10080 minutes to study the Amoxicillin release profile.After each reading, the aliquot was returned to the same bottle, so each measurement represents cumulative release [31, 32].

2.5.4) Paracetamol release profile studies:

The scaffolds coated with 1mg/mL paracetamol were immersed in PBS solution, and the Paracetamol release into PBS was noted at 196 nm at intervals 15 to 1140 minutes to study the Paracetamol release profile [33]. Aliquotes were returned to the bottle after reading.

2.5.5) Preparation of scaffold encapsulated with antibiotic-capped nHAp and painkiller.

20 mL of 8% sodium alginate solution was mixed with 20mg of Amoxicillin and 40 mg of nHAp. The mixture was crosslinked using chilled calcium chloride, and then lyophilised (as per the protocol given above) to prepare the scaffolds. The prepared scaffold was incubated for 1 day in a painkiller (Paracetamol) solution at a concentration of 1mg/mL. After incubation, the scaffolds were air-dried at room temperature.

2.5.6)Drug release studies for Amoxicillin and paracetamol integrated GTnHAp-alginate scaffold.

The scaffold integrated with amoxicillin and paracetamol was immersed in PBS solution for 10080 minutes and was analysed for drug release using ultraviolet-visible (UV-vis) spectrophotometry.

2.5.7)Release kinetics.

As the sampled aliquots were returned to the release medium after each reading, the measured concentrations represent cumulative release. Cumulative release (Q,%)was expressed relative to the maximum measured concentration of the individual profile, and the release phase (0 minutes up to the time of maximum release) was fitted by linear regression to zero-order (Q vs t), first order (log (100-Q) vs t), Higuchi (Q vs √t), Korsmeyer-Peppas (log Q vs log t), and Hixson-Crowell ($Q_0^{1/3} – Q_t^{1/3}$ vs t) models. The model with the highest coefficient of determination (R^2) was considered the best fit, and the Korsmeyer-Peppas release exponent (n) was

interpreted as Fickian diffusion ($n \leq 0.45$), anomalous transport ($0.45 < n < 0.89$) or Case II transport ($n \geq 0.89$) for a cylindrical matrix.

2.6) Biomineralization studies

A 100 mL solution of simulated body fluid (SBF) was prepared using the following reagents: 0.745 g NaCl, 0.044 g KCl, 0.035 g NaHCO3, 0.116 g CaCl2·2H2O, 0.031 g MgSO4·7H2O, 0.023 g Na2HPO4·2H2O, and 0.15 g Tris base. These reagents were dissolved in 90 mL of deionized water under constant magnetic stirring. The pH of the solution was adjusted to 7.4 using 1 M HCl. Subsequently, the solution was brought to a final volume of 100 mL with deionized water. Scaffolds embedded with Green tea nHAp were immersed in the prepared SBF solution. Following a designated incubation period (14 days), the SBF was aspirated, and the scaffolds were lyophilized and subjected to XRD and SEM analysis. The SEM analysis was carried out using an Ultra55 FE-SEM Carl Zeiss EDS [34].

2.7) Cytocompatibility assay

The 3-(4,5-dimethylthiazol-2-yl)-2,5-diphenyltetrazolium bromide (MTT) assay was carried out to evaluate the cytocompatibility of the cells after interacting with the scaffold samples:

- • nHAp + Alginate scaffold.
- •nHAp + Alginate + Amoxicillin scaffold.
- •nHAp+ Alginate + Amoxicillin + Paracetamol scaffold .

The MTT assay determines the extent to which viable cells can cause the conversion of tetrazolium in MTT to formazan. The assay was done on L929(Mouse fibroblast cell line), MG63 (Osteosarcoma cell line), and POB (Primary Osteoblast cells), which were cultured under standard culturing conditions.

Following a seeding density of 10^4 cells per well into 96-well plates, under sterile conditions, each scaffold formulation was kept immersed in full medium at 37 ∘C and 48 hours with agitation. The medium, consisting of the leachable components, was collected in a Falcon tube following the incubation period [35–36].Cell viability (%) was calculated as (absorbance of cells exposed to scaffold leachate /absorbance of untreated control cells) X 100.Untreated cells served as the 100% viability reference and a cytotoxic control was included in each assay.

2.8) FTIR analysis

The FTIR analysis was carried out for the nHAp-embedded alginate scaffold and the nHAp-embedded alginate scaffold integrated with paracetamol and an antibiotic. FTIR was carried out using a Perkin-Elmer Frontier FTIR spectrophotometer operating in the wavenumber range 4000 – 600 cm^{-1} to study whether the chemical integrity of the nHAp alginate scaffold was interfered with by the drugs integrated with the scaffold. The method followed was the ATR method [37, 38].

2.9) ALP analysis.

Alkaline Phosphatase(ALP) activity was carried out as an early marker of osteogenic differentiation using odontoblast-like cells (OLC), primary osteoblasts (POB), and their co-culture (OLC + POB) seeded onto pre-sterilised scaffolds and maintained under standard conditions in sustained growth medium. At specific time

intervals (Days 7,14 and 21), the cell-seeded scaffolds were removed from the culture plates and subjected to a PBS saline wash three times to ensure efficient residual medium removal.

Each scaffold was then treated with papain digestion buffer and incubated for 24 hours at 60ºC for proper digestion of the scaffold and release of the cellular contents. The digested samples were centrifuged, and the supernatant was collected for further analysis.

ALP content was determined using the SensoLyte® pNPP Alkaline Phosphatase Assay Kit (AnaSpec, USA) according to the prescribed protocol by the manufacturer. In a nutshell,50 µL of the sample supernatant was mixed with pNPP substrate and incubated at 37°C for an hour, during which pNPP was hydrolysed to p-nitrophenol by ALP, producing a yellow coloured product. Absorbance was measured at 405 nm using a microplate reader, and ALP content was calculated using a standard curve generated using the standards provided with the kit. To normalise the cell number difference, the DNA content of each sample was quantified using the Hoechst DNA assay. Final ALP values were given as ng of ALP /microgram of DNA (ng ALP/µg DNA) [39].

2.10) Antibacterial assay.

Alginate scaffolds integrated with green tea nHAp capped with amoxicillin were immersed in PBS solution for a period of 16 days. The scaffold leachates were collected on days 1,2,3,4,6,8,12 and 16 and tested for antibacterial activity by the agar diffusion method against *E. coli*, a Gram-negative model organism commonly used for primary screening of antibiotic-releasing biomaterials; Free amoxicillin was tested in parallel as the comparator. Plates were incubated for 24 hours at 37ºC, followed by measurement of the zone of inhibition as the radius from the centre of the well to the outer edge of the clear zone. The experiment was carried out in triplicate (n = 3), and results are expressed as mean ± standard deviation [40].

2.11) Statistical Analysis

Experiments were performed in triplicate (n = 3), and the results are presented as mean ± standard deviation (SD). Data processing and graphical visualization were performed using Microsoft Excel 2019 (Microsoft Corporation, Redmond, WA, USA) and OriginPro 9.0(OriginLab Corporation, Northampton, MA, USA). Swelling, degradation, drug release,cytocompatiblity,ALP activity and antibacterial data were analysed by two-way analysis of variance (ANOVA) followed by Tukey's HSD post hoc test; where groups were compared at individual time points,Tukey's HSD pooled within-group mean square from the ANOVA For the drug release studies, concentrations are expressed as mean ± Standard deviation (n = 3); two-way ANOVA (formulation x time)was performed excluding the 0-minute time point, and Tukey's HSD comparisons between formulations used the pooled within-group mean square from the ANOVA. Overall formulation means are presented as mean ± SE derived from the ANOVA model. A value of $p < 0.05$ was considered statistically significant.

3) Results and Discussion

3.1) Nanoparticle synthesis: Green synthesis of nanohydroxyapatite(nHAp).

nHAp was synthesized using green tea leaf extracts by the green synthesis protocol described in Section 2.2. The physicochemical and structural characterization of the synthesized nanoparticles was analysed using XRD to confirm successful synthesis before the fabrication of the scaffold.

3.1.1) Characterization of synthesized nHAp.

XRD of nHAp showed sharp peaks at crystal planes (002),(112), at 2θ = 26.0° and 32.1° respectively, these results are concurrent with the Joint Committee on Powder Diffraction Standards (JCPDS) standard PDF card No. 01-86-1199, confirming the formation of hydroxyapatite with a hexagonal crystal system (Fig. 1). The sharp, well-defined peaks indicate a high degree of crystallinity and long-range lattice order, attributed to the rapid, homogeneous nucleation facilitated by microwave-assisted synthesis [41]. The positions of peaks are consistent with values reported across HAp systems synthesized independently, in which peaks at 26º and 32.1º are indicators of well-crystallised,phase-pure hydroxyapatite[42].

The absence of secondary-phase peaks indicates that green tea polyphenols functioned as effective capping agents, modulating crystal growth without disrupting the lattice integrity[43]. This is significant, as phytochemical-mediated synthesis using green tea extract has been shown to promote chemical stability, osteogenic capacity, and antimicrobial properties of the nHAp, making it specifically suitable for dental tissue engineering applications [44]. Retaining high nHAp crystallinity is crucial for bone regeneration, as crystallised hydroxyapatite is dimensionally and chemically more stable, dissolves slowly and effectively under physiological conditions, and therefore retains a supersaturated calcium phosphate microenvironment that supports osteoblast attachment and ordered mineral deposition, instead of rapid, uncontrolled dissolution seen within poorly crystalline phases. The crystallographic characteristics observed here are consistent with prior literature, confirming the synthesis route and supporting the subsequent integration of synthesized nHAp into an alginate scaffold for dental bone tissue engineering.

3.2) Preparation of scaffold integrated with nanohydroxyapatite.

The green tea-mediated nanohydroxyapatite-integrated scaffold was fabricated according to the protocol described in Section 2.3.2. The structural and physicochemical characteristics of the nanocomposite scaffold were subsequently analysed using XRD, FTIR, and SEM to confirm the successful integration of nanohydroxyapatite within the alginate matrix before biological evaluation.

3.2.1) Optimization of the alginate concentrations.

The swelling properties of scaffolds containing 4%, 6%, and 8% alginate were analysed to determine the optimum polymer concentration for nanocomposite scaffold fabrication. Amongst the investigated formulations, the 8% scaffold showed the most favourable swelling property, along with maintaining structural integrity throughout the timeframe of the study. The improved performance of the 8% scaffold can be attributed to higher polymer concentration, forming a denser and more stable hydrogel network capable of retaining greater amounts of water without compromising scaffold integrity [13, 16]. Swelling property is crucial for tissue engineering scaffolds as it impacts nutrient diffusion, metabolite exchange, and the

maintenance of a hydrated microenvironment that supports tissue regeneration and cell survival [13, 16]. Optimisation considered not only swelling capacity but also the ability to preserve structural integrity and shape over the 15-day duration of the study, resistance to premature degradation, and the formation of a self-supporting, handleable lyophilised construct. The 4% and 6% alginate composite scaffolds swelled satisfactorily but lost integrity and were mechanically weaker; however, the 8% alginate composite scaffold balanced high uptake of water with structural stability. Based on this study, the 8% alginate composite scaffold was selected for further characterisation and evaluation studies.

3.3) Characterization of Scaffold.

3.3.1) XRD analysis.

The XRD of pure alginate shows a broad, diffuse peak instead of a well-defined, sharp peak. This characteristic is mainly due to the amorphous nature of the alginate (Fig. 2a). Such a structure is typical for natural polysaccharides like alginate, coinciding with the previously reported results for Sodium Alginate, which show a broad peak approximately in the 10–30º 2θ range. This amorphous behavior is advantageous for tissue engineering applications, as it often leads to flexibility and high porosity[45].

In contrast, the XRD results of the composite scaffold reveal sharp peaks at 32º, 45º, and 56º that correlate with the peaks of Crystalline nanohydroxyapatite. The retention of the broad background peaks further shows that the composite contains both alginate and crystalline HAp. This indicates successful integration of the nHAp into the alginate scaffold. This Combination of amorphous and crystalline nature demonstrates that the composite has the advantages of porosity and flexibility of the alginate, along with the bioactivity and structural integrity of the hydroxyapatite (Fig. 2b) [46].

3.3.2) SEM analysis

The SEM micrograph obtained at 10.00 KX magnification exhibited successful integration of Green tea-mediated nHAp within the alginate scaffold, indicating uniform distribution of almost spherical nanoparticles with minimal agglomeration (Fig. 3a). Higher magnification imaging at 50 kX resolved the individual nanohydroxyapatite sizes to be in the range of diameters ranging from 45.6–116.7 nm(Fig. 3b). These measurements validate the nanoparticle nature of the synthesized mineral phase and are consistent with nanoscale crystallites. The porous microstructure shows effective scaffold formation, offering a fluid-accessible architecture necessary for diffusion and waste exchange in bone tissue engineering [47]. Additionally, the homogeneous distribution of nHAp throughout the alginate matrix shows effective nanoparticle dispersion. This is functionally important, as uniform dispersion provides evenly distributed sites of nucleation for deposition of apatite, which agrees with the biomineralization results; also, limited agglomeration avoids the localised stress concentrations and heterogeneous degradation related to particle clustering.

3.3.3) Swelling analysis :

Swelling behaviour was analysed to quantify the fluid-uptake potential of the scaffolds and to evaluate how integration of green tea-mediated nHAp influences pore accessibility in comparison to the plain alginate

control. Water uptake impacts nutrient and metabolite diffusion through the construct and its dimensional stability in the moist state, both of which are necessary for cell infiltration in bone tissue engineering [48]. On the 11th day, the nHAp-integrated scaffold reached a swelling percentage of 421.85 ± 121.78% in comparison with 51.36 ± 13.2% for the alginate control.Two way ANOVA showed a significant effect of scaffold type ($F(1,24) = 219.36$, $p < 0.001$),with no significant effect of time ($F(5,24) = 1.10$,$p = 0.384$) or scaffold X time interaction ($F(5,24) = 0.59$,$p = 0.710$);Tukey's HSD confirmed that the nHAp-integrated scaffold swelled significantly more than the alginate control at every time point ($p < 0.001$).Mechanistically, the higher uptake in the composite is due to three crucial factors: the rich surface hydroxyl and phosphate groups of hydroxyapatite are strongly hydrophilic and create additional water-binding sites; the dispersed nanoparticles act as physical spacers that enhance capillary uptake and interconnected pore volume; and interfacial interaction between alginate carboxylate groups and nHAp loosens chain packing, allowing higher matrix expansion. An enhanced stable swelling capacity is biologically favourable as it improves nutrient and metabolite diffusion, cell infiltration during early tissue integration, and protein absorption. Together, these studies show that nHAp integration improved the swelling property of the scaffold. (Fig. 4a).

3.3.4) Degradation Analysis

Degradation of the scaffolds is a critical criterion for tissue engineering design. Preferably, the scaffold's degradation rate should be similar to the rate at which the new tissue forms to ensure proper functionalization of the newly formed tissue. Upon taking wet weights on Days 5, 7, 9, 11, and 15, it was observed that the scaffold weight increased for the first 24 hours for both the control (alginate) and the test (alginate + nHAp), and later started degrading. After day 9, it was found that the degradation was accelerated in the control, while the degradation in the test sample was happening at a controlled and slower pace. Upon calculating the degradation percentage at day 15, it was found that only the alginate scaffold had a higher degradation percentage (86.37 ± 2.01%) compared to the nHAp-integrated alginate scaffold (39.56 ± 2.70%), indicating that the addition of nHAp slowed down the degradation process of the scaffold. Two-way ANOVA confirmed significant effects of time ($F(4,20) = 104.29$,$p < 0.001$) and scaffold type ($F(1,20) = 10.73$,$p = 0.004$),and significant scaffold X time interaction ($F(4,20) = 34.88$,$p < 0.001$), reflecting this crossover. The slower degradation rate after integration of nanohydroxyapatite can be associated with the mineral phase reinforcing the network; nanohydroxyapatite-carboxylate interactions provide additional physical crosslink-like junctions that make the matrix stiff and hinder chain scission, as the buffering dissolution of apatite locally neutralises acidic degradation products, thus reducing the autocatalytic breakdown. Clinically, this controlled, elongated degradation is favourable as it keeps the scaffold structurally intact and mechanically stable over the weeks, which is essential for alveolar bone regeneration, so that the degradation rate of the scaffold is in sync with the rate of new tissue formation. From this study, we can validate that the integration of nanohydroxyapatite extends the degradation time of the fabricated scaffold (Fig. 4b).

Figure 4: Results for Swelling assay (a), Degradation assay(b) of Alginate and alginate scaffolds in PBS. Standard conditions maintained (pH = 7.4) at 37ºC over 15 days. Data are expressed as mean ± S.D. Significance levels: *$p < 0.05$, **$p < 0.01$, ***$p < 0.001$,**** $p < 0.0001$.Maximum swelling was observed on Day 11 and Maximum degradation was observed on day 15. Compared to pure alginate, the composite scaffold showed ▯370.49% points higher swelling on Day 11 and slowed degradation rate by ▯ 46.81% points on Day 15.

3.4) Drug loading and release studies.

3.4.1) Preparation of a standard curve for antibiotic and painkiller:

3.4.1.1) Antibiotic loading:

For the drug loading studies, the antibiotic drug Amoxicillin was chosen due to its extensive use as a dental antibiotic, and a working concentration of 1mg/mL was used.A standard curve of OD versus concentration (Fig. 5a) was prepared for 0.05-1.5mg/mL at 270 nm.

3.4.1.2) Painkiller loading:

For the drug loading, the painkiller chosen was Paracetamol, as it is one of the most commonly found and used painkillers in the market. A working concentration of 1mg/ml was used and a standard curve was prepared by measuring the absorbance of paracetamol solutions from 0.05 to 1.5 mg/ml at 196 nm (Fig. 5b).

3.4.2) Drug Release Profile:

Amoxicillin release profile.

The Amoxicillin release was found to be sustained in all three scaffolds (Fig. 5c,5e). The Amoxicillin-capped nHAp scaffolds reached an initial maximum at the 45th minute, with 1:2 (0.149 ± 0.035) giving higher release in comparison to 1:1 (0.113 ± 0.031 mg/mL). Both scaffolds attained a plateau by the 45th minute that was maintained for the rest of the 10080 minutes of the study. The highest concentrations were recorded at 1140 minutes for 1:2(0.150 ± 0.036 mg/mL) and at 1560 minutes for 1:1(0.127 ± 0.043 mg/mL), and the concentration at 10080 minutes (1:2: 0.143 ± 0.037 mg/ml;1:1: 0.119 ± 0.032 mg/mL) remained within 6% of the respective 45th minute values. This plateau shows the establishment of equilibrium partition between amoxicillin capped to the nHAp surface and the free amoxicillin in the solution, in agreement with the hydrogen-bonded, non-covalent drug-mineral association observed in FTIR analysis (Section 3.7). Throughout the study, the 1:2 formulation retained a higher mean release concentration (0.140 ± 0.005 mg/mL) in comparison to the 1:1 formulation (0.110 ± 0.005 mg/mL), showing that the amoxicillin-to-nanohydroxyapatite ratio impacts the antibiotic release. Two-way ANOVA validated a significant impact of formulation on the released amoxicillin concentration ($F(2,114) = 11.82, p < 0.001$), with no significant influence of time ($F(18,114) = 0.38, p = 0.989$) and no formulation X time interaction ($F(36,114) = 0.10, p > 0.999$). Tukey's HSD post hoc analysis indicated that the 1:1 formulation released significantly less amoxicillin than both the 1:2 formulation ($p < 0.001$) and the dual drug scaffold($p < 0.001$); the 1:2 formulation and the dual drug scaffold did not differ ($p = 0.819$)(Fig. 5c,e). Comparisons between formulations at individual points were not significant (all $p > 0.05$), owing to the replicate variability at each time point; the formulation difference arises from the consistent offset maintained across all time points. The absence of a time impact offers quantitative validation that the formulations maintained a stable plateau throughout the study time, while the significant formulation impact shows that the 1:2 ratio yields a consistently larger releasable reservoir.

Paracetamol release profile.

Paracetamol reached 0.859 ± 0.032 mg/mL within the first 15 minutes of the study, corresponding to 96% of its maximum release (0.897 ± 0.042 mg/mL at the 45th minute;n = 3). This indicates rapid availability as a

consequence of the surface coating strategy, as there is no polymeric barrier between the drug and PBS solution; release is impacted by immediate surface dissolution instead of diffusion through the alginate matrix. The concentration declined subsequently to 0.293 ± 0.029 mg/mL by the 150th minute and 0.090 ± 0.009 mg/mL by 1140 minutes (Fig. 5d); this decline does not represent a reduction in cumulative release, as sample aliquots were returned to the medium after each reading, and is associated with hydrolytic degradation of paracetamol in PBS buffer along with partial re-adsorption onto the scaffold surface.

Release from the dual-drug (amoxicillin and paracetamol) scaffold.

The dual-drug scaffold displayed the intended sequential release profile (Fig. 5e). Paracetamol reached 0.772 ± 0.031 mg/mL within 15 minutes (92% of its maximum of 0.840 ± 0.005 mg/mL at 45th minute) and then declined to 0.287 ± 0.024 mg/mL by the 150th minute and 0.031 ± 0.023 mg/mL by 10080 minutes, following the same pattern as the paracetamol-coated scaffold. Amoxicillin, in contrast, increased gradually from 0.110 ± 0.045 mg/mL at the 15th minute to a maximum release of 0.150 ± 0.037 mg/mL at the 1140th minute and remained at 0.121 ± 0.037 mg/mL (81% of the maximum)at the end of the study (10080 minutes). Amoxicillin release from the dual-drug scaffold was comparable to that of the 1:2 formulation, consistent with their identical amoxicillin-to-nHAp ratio, indicating that the paracetamol coating did not compromise the antibiotic reservoir.

Two-way ANOVA comparing paracetamol release from the paracetamol-coated and dual-drug scaffolds (15-1140 minutes)showed significant influence of formulation ($F(1,52) = 21.27, p < 0.001$), time ($F(12,52) = 1027.53, p < 0.001$), and formulation X time interaction ($F(12,52) = 2.05, p = 0.037$). Tukey's HSD showed that the dual-drug scaffold released less paracetamol during the initial burst at 15 ($p < 0.001$),30($p = 0.006$), and 45 minutes ($p = 0.003$), whereas the two scaffolds did not differ from 60 minutes onwards (all $p > 0.05$)(Fig. d,e). The overall mean paracetamol concentration was therefore slightly lower in the dual-drug scaffold(0.507 ± 0.004 mg/mL)than in the paracetamol-coated scaffold (0.531 ± 0.004 mg/ml; mean ± SE,n = 39 per formulation), with the difference confined to the burst phase. This may be attributed to the amoxicillin-capped nHAp in the dual-drug scaffold occupying surface sites otherwise available for paracetamol adsorption during the coating step; nevertheless,92% of the maximum paracetamol release was still achieved within 15 minutes, preserving the rapid analgesic phase.

3.4.3)Release mechanism and kinetics

The two drugs occupy structurally different compartments in the scaffold system, and this architectural variation is the basis of the noted release behaviour. Paracetamol is surface-coated onto the scaffold and has a rapid release as it only requires surface dissolution; however, amoxicillin, in contrast, has a sustained release as it is capped onto the nanohydroxyapatite and integrated into the alginate matrix, thus requiring dissociation from the nanohydroxyapatite and subsequent transport via the hydrated polymer network. Classical release models (Zero-order, First-order, Higuchi, Korsmeyer-Peppas, and Hixson-Crowell) were fitted to the release phase of each profile(Table 1). For the amoxicillin-capped nHAp scaffolds, none of the models described the profiles well ($R^2 \leq 0.65$ for 1:1 and ≤ 0.40 for 1:2); Korsmeyer-Peppas gave the highest R^2, with release exponents of 0.051(1:1) and 0.044(1:2), both far below the value of 0.45 characteristic of Fickian diffusion. For amoxicillin from the dual-drug scaffold, first-order kinetics gave the best fit ($R^2 = 0.876$), with a Korsmeyer-Peppas exponent of 0.075, reflecting its more gradual approach to the maximum. Zero-order, Higuchi, and

Korsmeyer-Peppas kinetics describe transport via a rate-limiting matrix and are formally applicable only to capped amoxicillin and not to surface-coated paracetamol; the paracetamol fits (best fit: Korsmeyer-Peppas, R^2 =0.986 for paracetamol-coated scaffold; first-order R^2 =1.000 for the dual-drug scaffold)are based on only three to four time points before the maximum at 45 minutes and are therefore not interpreted mechanistically. As 73–75% of the maximum amoxicillin release had already occurred by the first sampling point, beyond the ≤ 60% range for which the Korsmeyer-Peppas model is valid, these exponents are indicative rather than definitive. However, they are consistent with other observations like rapid attainment of a stable plateau within 45 minutes and the non-covalent mineral-drug interactions identified by FTIR, together indicating that the release is influenced by dissociation of amoxicillin from the nHAp surface instead of diffusional resistance of the alginate matrix, with the system acting as an equilibrium-buffered reservoir instead of a diffusional-controlled depot.

Table 1
Release kinetic model filling for amoxicillin and paracetamol release from the scaffolds. Fractional release was expressed relative to the maximum measured concentration, and models were fitted from 0 minutes to the time of maximum release

Scaffold(Drug)	Fitting window (min)	Zero-order R^2	First-order R^2	Higuchi R^2	Korsmeyer-Peppas	N	Hixson-Crowell R^2	Best fit
1:1 (amoxicillin)	0-1560	0.150	0.376	0.293	0.650	0.051	0.631	Korsmeyer-Peppas
1:2(amoxicillin)	0-1140	0.067	0.075	0.241	0.397	0.044	0.384	Korsmeyer-Peppas
Dual Drug (amoxicillin)	0-1140	0.089	0.876	0.308	0.790	0.075	0.490	First order
Paracetamol-coated (paracetamol)	0–45	0.634	0.947	0.867	0.986	0.040	0.881	Korsmeyer-Peppas
Dual drug (paracetamol)	0–45	0.665	1.000*	0.889	0.911	0.081	0.930	First order*

N,Korsmeyer-Peppas release exponent.*Fitted on three time points only, paracetamol fits are indicative and are not interpreted mechanistically.

3.5) Biomineralization studies.

Biomineralization studies were carried out to evaluate the scaffold's capacity to induce the formation of bone-like apatite on its surface, which validates that the scaffold is suitable for bone regeneration applications. Post-immersion XRD patterns of the nHAp-alginate scaffold showed that characteristic peaks at 2θ values of 27.5º, 31.9º, 45.8º, and 56.8º are consistent with the formation of crystalline hydroxyapatite (JCPDS 09-0432). These peaks correspond to the (002), (211), (222), and (511) crystallographic planes of hexagonal HA, respectively, confirming phase purity and bioactivity similar to bone mineral (Fig. 6a). The SEM image of a green tea nHAp-embedded alginate scaffold, following 14 days of incubation in simulated body fluid (SBF), shows a densely mineralized surface characterized by uniform deposition of apatite particles. This appreciable level of apatite

formation depicts the scaffold's enhanced bioactivity and ability to support mineral nucleation, highlighting its suitability for dental bone tissue engineering applications. Formation of apatite occurred because the exposed nanohydroxyapatite serves as a nucleation template; its surface Ca^{2+} and PO_4^{3-} sites lower the interfacial energy for heterogeneous nucleation, drawing phosphate and calcium ions from the SBF fluid to develop a bone-like apatite layer. This ability to induce calcium-phosphate nucleation is an in vitro hallmark of bioactivity and predicts osteoconductive properties in vivo, as the apatite layer formation mediates attachment to native bone and supports surface adhesion for the osteoblasts (Fig. 6b).

3.6) Cytocompatibility assay.

The cytocompatibility of the green tea-mediated nHAP-integrated scaffold and its drug-loaded formulations was evaluated by an MTT assay against MG63 osteoblastic like cells and Primary osteoblasts (POB) to evaluate osteogenic properties and L929 for safety evaluation. All formulations of scaffolds exhibited viability above the 70% non-cytotoxic threshold across all three cell types (Fig. 7a).MG63 viability was 96.69 ± 0.68%,97.81 ± 1.31% and 97.47 ± 1.17 for the nHAp-alginate scaffold, amoxicillin-capped nHAp integrated alginate scaffold, and paracetamol coated amoxicillin capped nHAp integrated alginate scaffold, L929 followed comparably (96.18 ± 1.50%,97.29 ± 1.42%,95.58 ± 0.66%), as did POB (92.23 ± 1.58%,93.36 ± 0.50%,92.93 ± 1.01%).Viability is shown relative to the untreated control (100.00 ± 1.20%);the cytotoxic control returned 3.03 ± 0.04%,validating the assay. Two way ANOVA indicated a significant impact of cell type ($F(2,18) = 37.50, p < 0.0001$)but no significant impact of formulation ($F(2,18) = 2.27$, $p = 0.132$) or cell type × formulation interaction ($F(4,18) = 0.45$, $p = 0.773$).Tukey's HSD validated that POB viability was lower in comparison to MG63 and L929 ($p < 0.0001$); however, no formulation pair varied significantly(Formulation main effect, all $p > 0.12$). Drug integration into the scaffold did not significantly impact the cytocompatibility. The values reported in this study are similar to those reported for comparable drug-loaded hydroxyapatite systems, which included ciprofloxacin -loaded nHAp(with > 95% viability under the same ISO criterion)[49] and an amoxicillin-loaded nanohydroxyapatite system, in which antibiotic integration led to no significant change in periodontal ligament stem cell proliferation [50]. Unlike single-drug systems, the present scaffold extends cytocompatibility to integrated antibiotic-analgesic delivery, further supporting its application in dental bone tissue engineering. Plain alginate was not included as a separate cytocompatibility control because its biocompatibility is well established [48] .

3.7) FTIR Analysis

FTIR was carried out to understand if the integration of drugs interferes with the chemical integrity of the scaffold. FTIR analysis of the nHAp-alginate scaffold and drug-loaded composites validated the successful integration of both scaffold components and drugs without compromising chemical integrity. Characteristic peaks at 3372 and 3351 cm^{-1} correspond to O–H/N–H stretching vibrations from alginate hydroxyl groups and structural water in nanohydroxyapatite. Specific peaks at 1633 and 1628 cm^{-1} represent asymmetric stretching of carboxylate groups in alginate, while phosphate peaks specific to nHAp appear near 1027–1028 cm^{-1} and 669–666 cm^{-1}. The integration of paracetamol and amoxicillin introduced additional bands at 1511 and 1410 cm^{-1}, typically aromatic C = C stretching and amide II vibrations from the drugs. Amoxicillin further contributes O–H and N–H stretches within 3200–3500 cm^{-1}, β-lactam and amide carbonyl stretches between 1800–1650 cm^{-1}, and N–H bending and C–N stretching in the range 1300–1250 cm^{-1}, while paracetamol shows amide C =

O and aromatic vibrations consistent with its structure. Apart from assigning peaks, the spectra also show how the components interact. The shift and slight broadening of the alginate O-H/carboxylate bands in the composite show hydrogen bonding and Ca2+-bridged electrostatic interaction between alginate carboxylate groups and the surface Ca^{2+}/OH^{-} belonging to nHAp, which is the physical source of the reinforced, slower degradation network observed above. The consistent characteristic amoxicillin peaks (β-lactam/amide) and paracetamol(amide/aromatic) bands without new covalent bands show the drugs are held by hydrogen bonding and physical entrapment instead of other stronger chemical bonds. The lack of peak loss or new covalent bond formation validates that the drug loading retains the chemical integrity of the scaffold, confirming its structural stability and supporting its application in dental tissue engineering and for controlled drug delivery(Fig. 8)[51–53].

3.8) ALP Activity.

Alkaline phosphatase is an ectoenzyme bound to the osteoblast membrane that hydrolyses inorganic pyrophosphate, an inhibitor of hydroxyapatite nucleation, thereby allowing mineral deposition in the collagen matrix. Its increment indicates the transition from proliferation to matrix maturation and precedes late markers like osteocalcin, so ALP is interpreted here as a functional index of differentiation state instead of cell number.

ALP activity varied significantly amongst the groups at and over time(two-way ANOVA:cell type $F(2,18) = 3447.96$,time $F(2,18) = 23424.73$,cell type X time interaction $F(4,18) = 238.08$;all $p < 0.0001$;Fig. 7b).At the 7th day, values were 120.20 ± 2.83,150.32 ± 3.76 and 220.01 ± 6.92 ng ALP/µg DNA for OLC, POB and OLC + POB, increasing to 540.28 ± 3.18, 600.48 ± 4.54 and 800.22 ± 6.62 ng ALP/µg DNA by the 21st day(Fig. 7b).

Pairwise comparisons between cell types were significant at every time point (Tukey's $p < 0.0001$;Fig. 7b). The co-culture showed the highest ALP activity at every time point, indicating accelerated entry into matrix maturation.

These results are concurrent with the alginate-based systems in rank order, though not in kinetics. Alipour et al.,2021[54] reported 2.7 times and 3times higher ALP in alginate-gelatin and alginate/nanohydroxyapatite microcapsules than the 2-dimensional control on the 21st day, with nanohydroxyapatite significantly superior to the nanohydroxyapatite-free formulation. *Sancilio et al. 2018* [55] contrarily found ALP in Dental pulp stem cells (DPSCs) on freeze-dried alginate integrated with nanohydroxyapatite scaffolds peaked at day 3 and fluctuated weakly after that, possibly indicating differences in cell type, scaffold architecture, and culture duration. Normalisation differences limit direct numerical comparison.

However, both studies differed in scaffold formulation at fixed cell type; here, at fixed formulation, the co-culture raised ALP 1.33-fold over POB by 21st day. This is most probably attributed to the bidirectional paracrine signalling, with odontoblast-derived dentin matrix protein-1 (DMP-1) and bone morphogenic protein-2 (BMP-2) leading to Runt-related transcription factor 2 (Runx2)-dependent expression of ALP, mimicking the native dentine-bone interface more truly than monoculture. As ALP was measured only on the nHAp-alginate scaffold, these data show that the scaffold supports ALP activity of the three cell populations; they do not isolate the specific contribution of nHAp, which would require comparison with nHAp-free alginate and tisuue culture controls (section 3.10).The contribution of nHAp was,however established for the physical properties of the scaffold,with higher swelling and lower mass loss than plain alginate (Section 3.3.3.3 and 3.3.34) and

nHAp integration into alginate has previously been shown to increase ALP activity relative to nHAp-free alginate [54]

3.9)Antibacterial activity.

The amoxicillin-capped nHAp integrated alginate scaffold showed significantly higher antibacterial activity against *E.coli* in comparison to the free amoxicillin through the early release phase (Day 1–6, Tukey's HSD,$p < 0.05$). The zone of inhibition for the scaffold was found to be maximum on Day 6 (1.70 ± 0.20 cm), which was compared to that of free Amoxicillin (0.23 ± 0.12cm). The free Amoxicillin gives a rapid release and hence has an almost constant zone of inhibition throughout the time duration of the studies; however, the phasic release of the amoxicillin from the scaffold contributes to the increment of the zone of inhibition during the early phase of the experiment (Day 1-Day 6). Beyond Day 6, the zone sharply declined and almost became similar to that of the free amoxicillin (Days 8–16,$p > 0.05$). The decline in the zone of inhibition post-Day 6 can be due to the depletion of loosely capped amoxicillin, which leads to a lower concentration of amoxicillin in the leachate post-Day 6.Two-way ANOVA validated significant impacts of formulation ($F(1,32) = 105.16$),time ($F(7,32) = 19.54$) and their interaction ($F(7,32) = 18.99$;all $p < 0.001$), showing that release-dependent activity was impacted by both the scaffold and the elution time. The sustained early-phase inhibition relative to free amoxicillin is explained by the release mechanism, that is, capping the antibiotic onto nHAp and integrating it into the alginate matrix, which retains the drug through reversible, non-covalent binding to the mineral so that an equilibrium reservoir rather than a single burst,influences its availability. This maintains an inhibitory local concentration over the time period, hence widening the inhibition zone during the phase when risk of infection is highest; free amoxicillin depletes almost immediately. The relation between the sustained release profile and the Day 1 to Day 6 inhibition zones validates that the nHAp-mediated modulation of release, not only the total drug load, drives the enhanced antibacterial efficiency. The sustained early-phase zone of inhibition indicates that nanohydroxyapatite integration modulated amoxicillin release, prolonging the therapeutically active window relative to free drug [56, 57]. The decline at later phases likely shows depletion of the loaded antibiotic reservoir (Fig. 9).The antibacterial activity was confirmed against *E.coli* as a model organism:evaluation against oral pathogens (e.g.,*Streptococcus mutans*, *Enterococcus faecalis* and *Porphyromonas gingivalis*)will be undertaken in future studies.

Figure 9: Antibacterial assay carried out on nHAp-alginate scaffold integrated with amoxicillin compared against free amoxicillin. The graph is represented as mean ± SD (n = 3). The scaffold integrated with amoxicillin is found to have given a bigger zone of inhibition on day 6 (1.70 ± 0.20 cm), indicating sustained amoxicillin release, in comparison to the free amoxicillin, which gave a burst release and a smaller zone of inhibition (0.23 ± 0.12 cm on day 6). Significance levels: *$p < 0.05$, **$p < 0.01$, ***$p < 0.001$,****$p < 0.0001$;Days 8–16 not significant.

4) Conclusion

Traumatic dental tissue, being a global health concern, impacts a spectrum of age groups globally, highlighting the significance of personalised therapies to treat it. Dental tissue engineering offers personalized treatments that cater to patient-specific needs. This study advances dental bone tissue engineering by exhibiting that green synthesis (phytochemical-mediated synthesis), osteogenesis for bone regeneration, and phase-specific dual drug delivery functionality are unified into a single fabricated scaffold. Instead of treating inflammation,

infection, and bone loss as individual problems, the platform tackles them concurrently while remaining free of toxic reagents, overall making it unique from the previous single-function or simultaneous release systems. The combination of customisable degradation, apatite-forming bioactivity, phase-specific release, enhanced ALP activity, and cytocompatibility indicates a scaffold's capacity to support the sequence of events essential for alveolar bone healing post-trauma. Implementing clinical translation will require more work in the areas of mechanical characterization under physiologically relevant loading, quantification of total drug loading and drug release under physiologically relevant dynamic conditions, and in vivo validation in animal models to confirm safe degradation, osteogenesis, and infection control, followed by studies leading towards clinical use. The modular design also allows the drug pair to be customised to specific dental and craniofacial applications.

Declarations

Funding

The authors did not receive any funding support from any organisation for the submitted work.

Competing interests

The Authors have no relevant financial or non-financial interests to disclose.

Author contributions:

Ananya N. Nayak: Conceptualization, Methodology, Investigation, Supervision, Formal analysis, Data curation, Visualization, Writing – original draft.

Roshni Ramachandran: Conceptualization, Validation, Supervision, Visualization, and Writing – review & editing.

Hansel P. Shah: Investigation, Data curation.

Ishani Chowdhary: Investigation, Data curation.

Punya Sharma: Investigation, Data curation.

Ethics approval

Not applicable :commercially obtained cell lines only.

Consent to participate/Consent to publish :

Not applicable.

Data availability

Made available on request from the corresponding author.

References

1. L.V. Reddy, R. Bhattacharjee, E. Misch, M. Sokoya, Y. Ducic, Dental injuries and management. Facial Plast. Surg. **35**(6), 607–613 (2019). https://doi.org/10.1055/s-0039-1700877
2. S. Petti, J.O. Andreasen, U. Glendor, L. Andersson, NA0D – the new traumatic dental injury classification of the World Health Organization. Dent. Traumatol. **38**(3), 170–174 (2022). https://doi.org/10.1111/edt.12753
3. L. Mordini, P. Lee, R. Lazaro, R. Biagi, L. Giannetti, Sport and dental traumatology: surgical solutions and prevention. Dent. J. **9**(3), 33 (2021). https://doi.org/10.3390/dj9030033
4. C. Bourguignon, N. Cohenca, E. Lauridsen, M.T. Flores, A.C. O'Connell, P.F. Day et al., International Association of Dental Traumatology guidelines for the management of traumatic dental injuries: 1. Fractures and luxations. Dent. Traumatol. **36**(4), 314–330 (2020). https://doi.org/10.1111/edt.12578
5. R. Gruber, Osteoimmunology: Inflammatory osteolysis and regeneration of the alveolar bone. J. Clin. Periodontol. **46**, 52–69 (2019). https://doi.org/10.1111/jcpe.13056
6. M. Saleh Hasani Jebelli, A. Yari, N. Nikparto, S. Cheperli, A. Asadi, A.A. Darehdor et al., Tissue engineering innovations to enhance osseointegration in immediate dental implant loading: A narrative review. Cell. Biochem. Funct. **42**(2), e3974 (2024). https://doi.org/10.1002/cbf.3974
7. V. Rosa, A. Della Bona, B.N. Cavalcanti, J.E. Nör, Tissue engineering: from research to dental clinics. Dent. Mater. **28**(4), 341–348 (2012). https://doi.org/10.1016/j.dental.2011.11.025
8. A. Machado, I. Pereira, J.E. Pereira, L. Maltez, A. Brandão, R. Alvites et al., Dextrin hydrogel loaded with a macroporous Bonelike® scaffold and dental pulp stem cells for critical-sized defect repair. Materialia. **30**, 101859 (2023). https://doi.org/10.1016/j.mtla.2023.101859
9. J. Sun, C. Chen, B. Zhang, C. Yao, Y. Zhang, Advances in 3D-printed scaffold technologies for bone defect repair: materials, biomechanics, and clinical prospects. Biomed. Eng. Online. **24**(1), 51 (2025). https://doi.org/10.1186/s12938-025-01381-w
10. Z. Terzopoulou, A. Zamboulis, I. Koumentakou, G. Michailidou, M.J. Noordam, D.N. Bikiaris, Biocompatible synthetic polymers for tissue engineering purposes. Biomacromolecules. **23**(5), 1841–1863 (2022). https://doi.org/10.1021/acs.biomac.2c00047
11. D.T. Wu, J.G. Munguia-Lopez, Y.W. Cho, X. Ma, V. Song, Z. Zhu, S.D. Tran, Polymeric scaffolds for dental, oral, and craniofacial regenerative medicine. Molecules. **26**(22), 7043 (2021). https://doi.org/10.3390/molecules26227043
12. D. Yang, J. Xiao, B. Wang, L. Li, X. Kong, J. Liao, The immune reaction and degradation fate of scaffold in cartilage/bone tissue engineering. Mater. Sci. Eng. C **104**, 109927 (2019). https://doi.org/10.1016/j.msec.2019.109927
13. F. Zhang, M.W. King, Biodegradable polymers as the pivotal player in the design of tissue engineering scaffolds. Adv. Healthc. Mater. **9**(13), 1901358 (2020). https://doi.org/10.1002/adhm.201901358
14. B. Özcolak, B. Erenay, S. Odabaş, K.D. Jandt, B. Garipcan, Effects of bone surface topography and chemistry on macrophage polarization. Sci. Rep. **14**(1), 12721 (2024). https://doi.org/10.1038/s41598-024-62484-3
15. T. Chen, Y. Jiang, J.P. Huang, J. Wang, Z.K. Wang, P.H. Ding, Essential elements for spatiotemporal delivery of growth factors within bio-scaffolds: a comprehensive strategy for enhanced tissue regeneration. J. Control Release. **368**, 97–114 (2024). https://doi.org/10.1016/j.jconrel.2024.02.006

16. D.R. Sahoo, T. Biswal, Alginate and its application to tissue engineering. SN Appl. Sci. **3**(1), 30 (2021). https://doi.org/10.1007/s42452-020-04096-w
17. S.U. Rahman, Hydroxyapatite and tissue engineering. In: Handbook of Ionic-Substituted Hydroxyapatites. Woodhead Publishing. 383–400 (2020). https://doi.org/10.1016/B978-0-08-102834-6.00016-1
18. S. Singh, A. Pal, S. Mohanty, Nanostructure of hydroxyapatite and its modern approach in pharmaceutical science. Res. J. Pharm. Technol. **12**(3), 1463–1472 (2019). https://doi.org/10.5958/0974-360X.2019.00243.9
19. A. Siriphap, A. Kiddee, A. Duangjai, A. Yosboonruang, G. Pook-In, S. Saokaew et al., Antimicrobial activity of the green tea polyphenol (–)-epigallocatechin-3-gallate (EGCG) against clinical isolates of multidrug-resistant Vibrio cholerae. Antibiotics. **11**(4), 518 (2022). https://doi.org/10.3390/antibiotics11040518
20. A.D. VK, S. Ray, U. Arora, S. Mitra, A. Sionkowska, A.K. Jaiswal, Dual drug delivery platforms for bone tissue engineering. Front. Bioeng. Biotechnol. **10**, 969843 (2022). https://doi.org/10.3389/fbioe.2022.969843
21. D. Govindaraj, M. Rajan, Synthesis and spectral characterization of novel nano-hydroxyapatite from Moringa oleifera leaves. Mater. Today Proc. 3(6), 2394–2398 (2016). https://doi.org/10.1016/j.matpr.2016.04.153
22. A. Vijayalekha, H. Sridhar, S. Srinivasan et al., Integrative network pharmacology and experimental validation of rutin-infused collagen–hydroxyapatite scaffold for promoting osteochondral regeneration. 3 Biotech. **15**, 290 (2025). https://doi.org/10.1007/s13205-025-04461-9
23. T. Shi, Q. Li, D. Zhao, B. Zhong, H. Xu, L. Chen et al., 3D-Printed lithium disilicate-resin composites with bioinspired toughening radial-concentric architecture for dental restorations. Dent. Mater. (2026). https://doi.org/10.1016/j.dental.2026.05.012
24. V. Jayachandran, S.S. Murugan, P.A. Dalavi, Y.D. Vishalakshi, G.H. Seong, Alginate-based composite microspheres: preparations and applications for bone tissue engineering. Curr. Pharm. Des. **28**(13), 1067–1081 (2022). https://doi.org/10.2174/1381612828666220518142911
25. J.A.R. Pasqual, da A.P.B. Silva, N.B. Guerra, C.C. Schmitt, 3D-printed multifunctional PLA scaffolds with polyvinylidene fluoride, hydroxyapatite, and 45S5 bioactive glass. Biomed. Mater. Devices. (2026). https://doi.org/10.1007/s44174-026-00753-7
26. K. Seethalakshmi, M. Kaviya, B. Venkatachalapathy, S. Mubeena, A.M. Punnoose, T.Á. Sridhar, Nanohydroxyapatite-doped polycaprolactone-based nanoscaffolds as a viable drug delivery agent in bone tissue engineering. J. Mater. Res. **36**(2), 420–430 (2021). https://doi.org/10.1557/s43578-020-00042-z
27. N. Singh, I.J. Das, S. Satpathi, D. Das, B.S. Patro, K. Jena et al., Drug release potential of polyacrylamide grafted-Assam Bora rice polysaccharide graft copolymer (ABRS-g-PAM) as effective controlled release polymer. Carbohydr. Res. **549**, 109355 (2025). https://doi.org/10.1016/j.carres.2024.109355
28. H.M. Abdel-Mageed, A.E. Aziz, A.E. Abdel Raouf, Antioxidant-biocompatible and stable catalase-based gelatin–alginate hydrogel scaffold with thermal wound healing capability: immobilization and delivery approach. 3 Biotech. **12**, 73 (2022). https://doi.org/10.1007/s13205-022-03131-4
29. C. Turemis, G. Baysan, S. Aydemir, O. Colpankan Gunes, R.B. Husemoglu, H. Ates, M. Perpelek, A. Ziylan Albayrak, B. Baykara, S. Surucu, B. Cecen, H. Havitcioglu, Hydroxyapatite and loofah-reinforced carboxymethyl chitosan hydrogel scaffold with/without stem cells for bone healing: in vitro and in vivo. Biomed. Mater. Devices. (2025). https://doi.org/10.1007/s44174-025-00565-1

30. S. Kumari, B.N. Singh, P. Srivastava, Effect of copper nanoparticles on physico-chemical properties of chitosan and gelatin-based scaffold developed for skin tissue engineering application. 3 Biotech. **9**, 102 (2019). https://doi.org/10.1007/s13205-019-1624-9
31. X. Mo, D. Zhang, K. Liu, X. Zhao, X. Li, W. Wang, Nano-hydroxyapatite composite scaffolds loaded with bioactive factors and drugs for bone tissue engineering. Int. J. Mol. Sci. **24**(2), 1291 (2023). https://doi.org/10.3390/ijms24021291
32. E. Güncüm, N. Işıklan, C. Anlaş, N. Ünal, E. Bulut, T. Bakırel, Development and characterization of polymeric-based nanoparticles for sustained release of amoxicillin–an antimicrobial drug. Artif. Cells Nanomed. Biotechnol. **46**(sup2), 964–973 (2018). https://doi.org/10.1080/21691401.2018.1476371
33. N.T.T. Uyen, Z.A.A. Hamid, N.B. Ahmad, Synthesis and characterization of curcumin-loaded alginate microspheres for drug delivery. J. Drug Deliv Sci. Technol. **58**, 101796 (2020). https://doi.org/10.1016/j.jddst.2020.101796
34. G. Strömberg, L. Aalto-Setälä, P. Uppstu, R. Björkenheim, J. Pajarinen, E. Eriksson, N.C. Lindfors, L. Hupa, Development and characterization of non-coated and PLGA-coated S53P4 and S59 bioactive glass scaffolds for treatment of load-bearing defects. Biomed. Mater. Devices. **2**, 498–509 (2024). https://doi.org/10.1007/s44174-023-00099-4
35. S. Anitha, S. Shivakumar, Transparent keratin nanocomposite films incorporating silver nanoparticles and aloe vera for wound management. 3 Biotech. **16**(7), 286 (2026). https://doi.org/10.1007/s13205-026-04908-7
36. X. Qiu, X. Liu, Y. Qi, Y. Zhang, C. Zhou, J. Wu, Novel dual-capsule dental resin for crack-sensing, self-healing and self-warning. Dent. Mater. (2026). https://doi.org/10.1016/j.dental.2026.03.153
37. M.I. Hassan, N. Sultana, Characterization, drug loading and antibacterial activity of nanohydroxyapatite/polycaprolactone (nHA/PCL) electrospun membrane. 3 Biotech. **7**(4), 249 (2017). https://doi.org/10.1007/s13205-017-0889-0
38. D.G. Miranda, S.M. Malmonge, D.M. Campos, N.G. Attik, B. Grosgogeat, K. Gritsch, A chitosan-hyaluronic acid hydrogel scaffold for periodontal tissue engineering. J. Biomed. Mater. Res. B Appl. Biomater. **104**(8), 1691–1702 (2016). https://doi.org/10.1002/jbm.b.33516
39. B. Gurumurthy, P. Pal, J.A. Griggs, A.V. Janorkar, Optimization of collagen-elastin-like polypeptide-bioglass scaffold composition for osteogenic differentiation of adipose-derived stem cells. Materialia. **9**, 100572 (2020). https://doi.org/10.1016/j.mtla.2019.100572
40. R. Raju, D. Prakash, A. Jayaraman, B.V. Basavaraj, M.J. Darshan, In situ nanocrystalline silver chloride embedded xanthan–alginate scaffold with synergistic antimicrobial activity and rapid wound repair. 3 Biotech. **16**(9), 372 (2026). https://doi.org/10.1007/s13205-026-05011-7
41. M. Irfan, A. Jeshurun, B.M. Reddy, Microwave-assisted synthesis of dual responsive luminomagnetic rare earth metal ions (Nd3+, Dy3+) co-doped nanohydroxyapatite for biomedical applications. Dalton Trans. **54**(9), 3774–3795 (2025). https://doi.org/10.1039/D4DT02664K
42. S. Shaikh, S. Gupta, A. Mishra, P.A. Sheikh, P. Singh, A. Kumar, Laser-assisted synthesis of nano-hydroxyapatite and functionalization with bone active molecules for bone regeneration. Colloids Surf. B Biointerfaces. **237**, 113859 (2024). https://doi.org/10.1016/j.colsurfb.2024.113859

43. N.K. Daimari, A. Gogoi, R. Biswas, N. Mazumder, Role of solvents in iron nanoparticle synthesis: analyzing water and 1-methyl-2-pyrrolidone with green tea extract as a reducing agent. ACS Omega. **10**(28), 30985–30995 (2025). https://doi.org/10.1021/acsomega.5c03914
44. P. Ilancheran, J. Paulraj, S. Maiti, R. Shanmugam, Green synthesis, characterization, and evaluation of the antimicrobial properties and compressive strength of hydroxyapatite nanoparticle-incorporated glass ionomer cement. Cureus. **16**(4), e58562 (2024). https://doi.org/10.7759/cureus.58562
45. C. Larosa, M. Salerno, de J.S. Lima, R.M. Meri, da M.F. Silva, de L.B. Carvalho, A. Converti, Characterisation of bare and tannase-loaded calcium alginate beads by microscopic, thermogravimetric, FTIR and XRD analyses. Int. J. Biol. Macromol. **115**, 900–906 (2018). https://doi.org/10.1016/j.ijbiomac.2018.04.138
46. I. Mobasherpour, M.S. Heshajin, A. Kazemzadeh, M. Zakeri, Synthesis of nanocrystalline hydroxyapatite by using precipitation method. J. Alloys Compd. **430**, 330–333 (2007). https://doi.org/10.1016/j.jallcom.2006.05.018
47. Z. Feyisa, N.K. Gupta, G.D. Edossa, A. Sundaramurthy, A. Kapoor, L.G. Inki, Fabrication of pH-sensitive double cross-linked sodium alginate/chitosan hydrogels for controlled release of amoxicillin. Polym. Eng. Sci. **63**(8), 2546–2564 (2023). https://doi.org/10.1002/pen.26395
48. K.Y. Lee, D.J. Mooney, Alginate: properties and biomedical applications. Prog Polym. Sci. **37**(1), 106–126 (2012). https://doi.org/10.1016/j.progpolymsci.2011.06.003
49. M.B. Mobarak, F. Chowdhury, M.N. Uddin, M.S. Hossain, U.S. Akhtar, N.I. Tanvir et al., Poultry waste derived in situ drug loaded nano-hydroxyapatite bio-ceramic material for osteomyelitis treatment: in vitro drug release and biocompatibility studies. Mater. Adv. **5**(24), 9716–9730 (2024). https://doi.org/10.1039/d4ma00748d
50. X. Xiong, A. Li, Z. Zhang, Z. Wang, H. Chen, L. Guo, In vitro study on the bacteriostatic effect of Amoxicillin-loaded Nano-hydroxyapatite and its capability in occluding dentinal tubules. Sci. Rep. **15**(1), 41211 (2025). https://doi.org/10.1038/s41598-025-25128-8
51. D. Liu, Z. Liu, J. Zou, L. Li, X. Sui, B. Wang et al., Synthesis and characterization of a hydroxyapatite–sodium alginate–chitosan scaffold for bone regeneration. Front. Mater. **8**, 648980 (2021). https://doi.org/10.3389/fmats.2021.648980
52. D.A. Gaber, H.S. Alhawas, F.A. Alfadhel, S.A. Abdoun, A.M. Alsubaiyel, R.M. Alsawi, Mini-tablets versus nanoparticles for controlling the release of amoxicillin: in vitro/in vivo study. Drug Des. Dev. Ther. **14**, 5405–5418 (2020). https://doi.org/10.2147/DDDT.S285522
53. S. Fanelli, A. Zimmermann, E.G. Totoli, H.R.N. Salgado, FTIR spectrophotometry as a green tool for quantitative analysis of drugs: practical application to amoxicillin. J. Chem. 2018, 3920810 (2018). https://doi.org/10.1155/2018/3920810
54. M. Alipour, N. Firouzi, Z. Aghazadeh, M. Samiei, S. Montazersaheb, A.B. Khoshfetrat, M. Aghazadeh, The osteogenic differentiation of human dental pulp stem cells in alginate-gelatin/Nano-hydroxyapatite microcapsules. BMC Biotechnol. **21**(1), 6 (2021). https://doi.org/10.1186/s12896-020-00666-3
55. S. Sancilio, M. Gallorini, Di C. Nisio, E. Marsich, Di R. Pietro, H. Schweikl, A. Cataldi, Alginate/hydroxyapatite-based nanocomposite scaffolds for bone tissue engineering improve dental pulp biomineralization and differentiation. Stem Cells Int. 2018, 9643721 (2018). https://doi.org/10.1155/2018/9643721

56. H. Manzoor, N. Arshad, M.A. Ur Rehman Qureshi, A. Javed, Hydroxyapatite-reinforced pectin hydrogel films PEC/PVA/APTES/HAp: doxycycline loading for sustained drug release and wound healing applications. RSC Adv. **15**(37), 30026–30045 (2025). https://doi.org/10.1039/d5ra01989c
57. J. Prakash, T. Sushil Kumar, K.S. Venkataprasanna, R. Niranjan, M. Kaushik, D.B. Samal, G.D. Venkatasubbu, PVA/alginate/hydroxyapatite films for controlled release of amoxicillin for the treatment of periodontal defects. Appl. Surf. Sci. **495**, 143543 (2019). https://doi.org/10.1016/j.apsusc.2019.143543

Figures

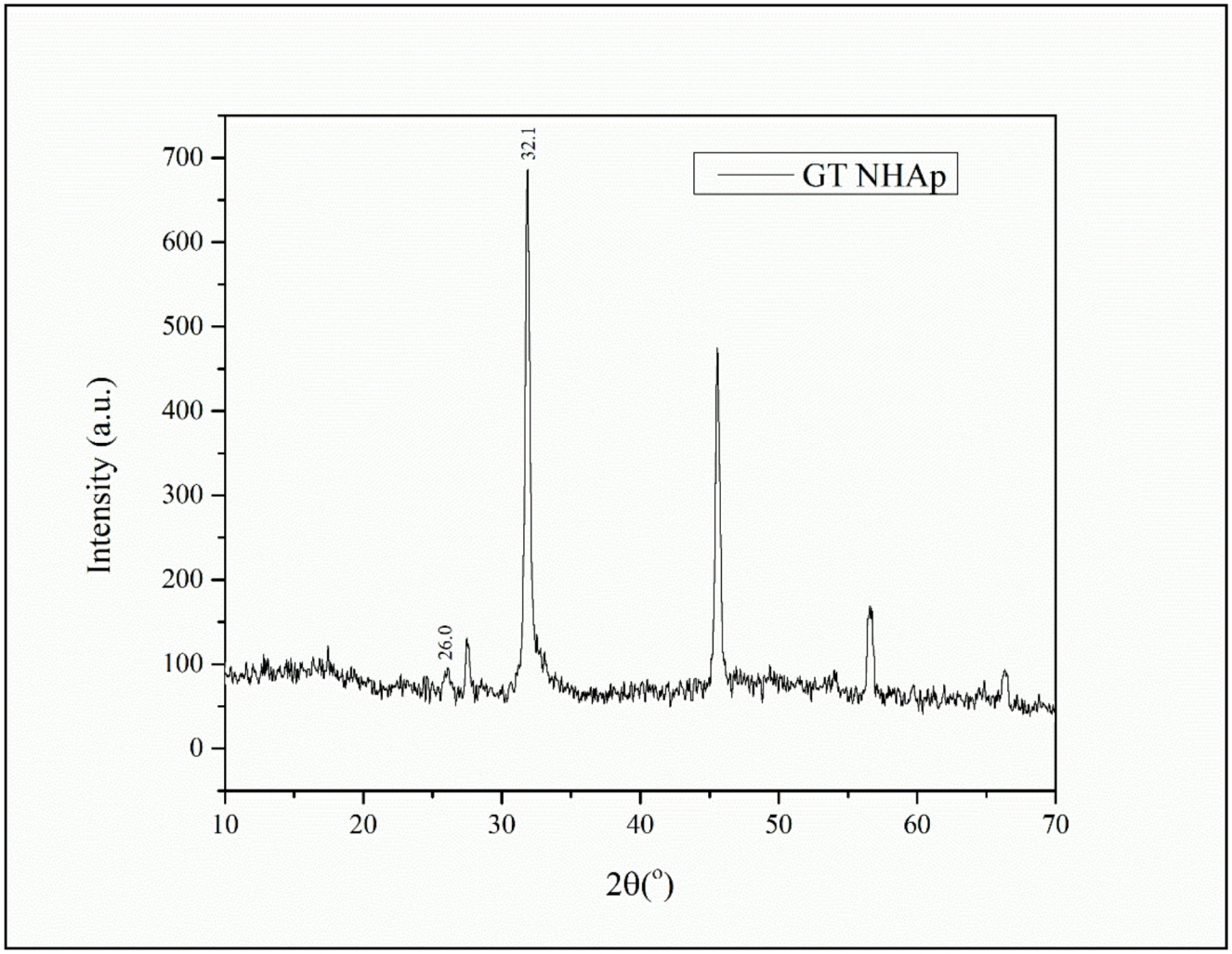


Figure 1

XRD pattern of nHAp synthesized using green tea leaves extract. Sharp peaks at 2θ=26.0º and 32.1º, corresponding to the (002) and (112) crystal planes, confirm the formation of hydroxyapatite with hexagonal crystal system,, indexed to JCPDS PDF card number 01-86-1199.The sharpness and definition of the peaks indicate high crystallinity and long-range lattice order.

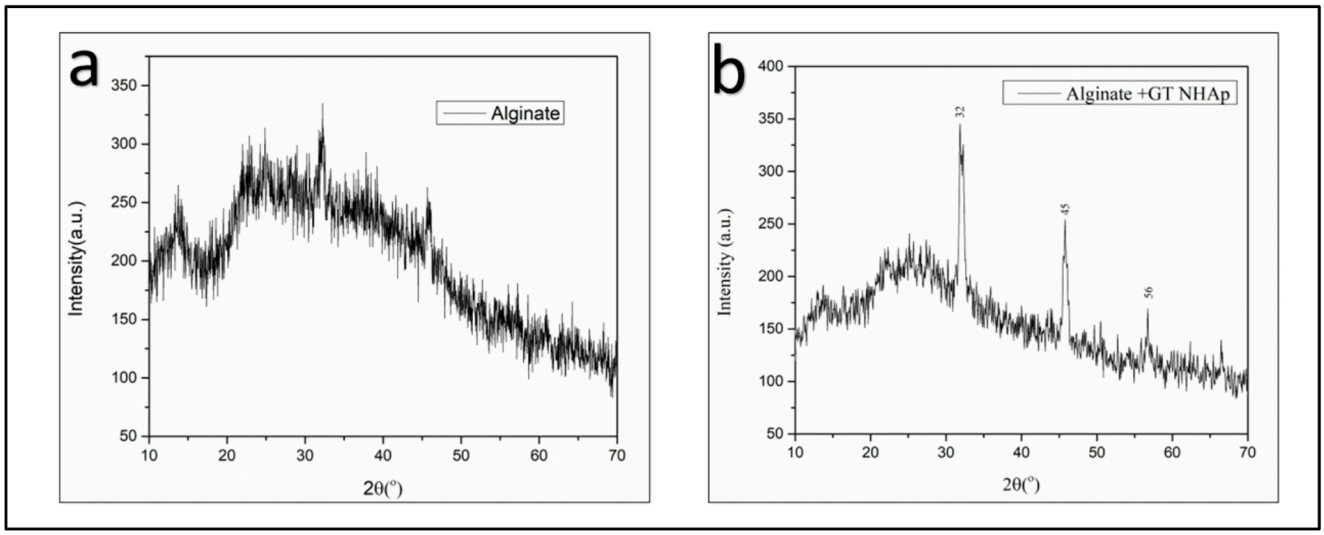


Figure 2

XRD pattern of alginate (a) and green tea-mediated nanohydroxyapatite-integrated alginate scaffold(b). Pure alginate indicates a broad, diffuse peak in the 2θ=10-30º range, characteristic of its amorphous nature; however, the composite exhibits sharp crystalline nHAp reflections at 2θ=32º, 45º and 56º superimposed on the retained amorphous background, confirming successful integration of nHAp within the alginate matrix.

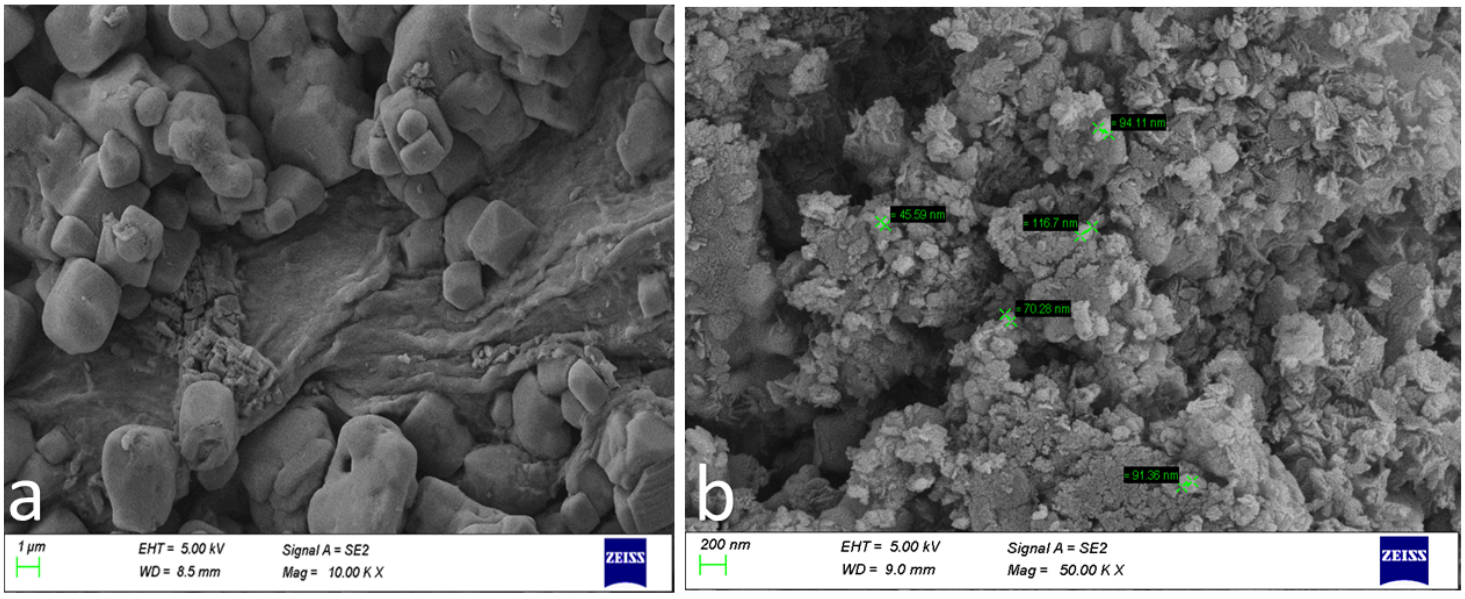


Figure 3

SEM micrographs of the nHAp-integrated scaffold .(a)Surface morphology at 10.00kX showing nHAp embedded within the alginate matrix;(b) nHAp particles at 50.00kX with representative Feret diameters (45.6-116.7 nm). EHT=5.00 kV, WD=8.5mm (a) and 9.0 mm(b): scale bars,1µm (a) and 200 nm (b).

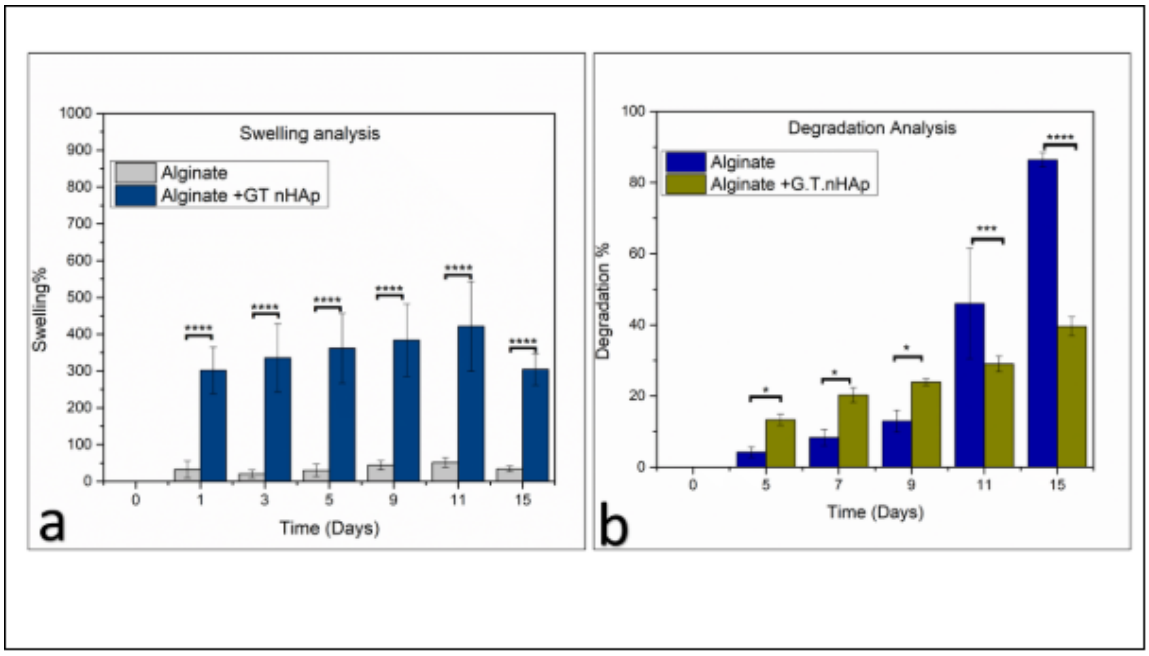


Figure 4

Results for Swelling assay (a), Degradation assay(b) of Alginate and alginate scaffolds in PBS . Standard conditions maintained (pH=7.4) at 37ºC over 15 days. Data are expressed as mean ± S.D. Significance levels: *p < 0.05, **p < 0.01, ***p < 0.001,**** p<0.0001.Maximum swelling was observed on Day 11 and Maximum degradation was observed on day 15. Compared to pure alginate, the composite scaffold showed 370.49 % points higher swelling on Day 11 and slowed degradation rate by 46.81% points on Day 15.

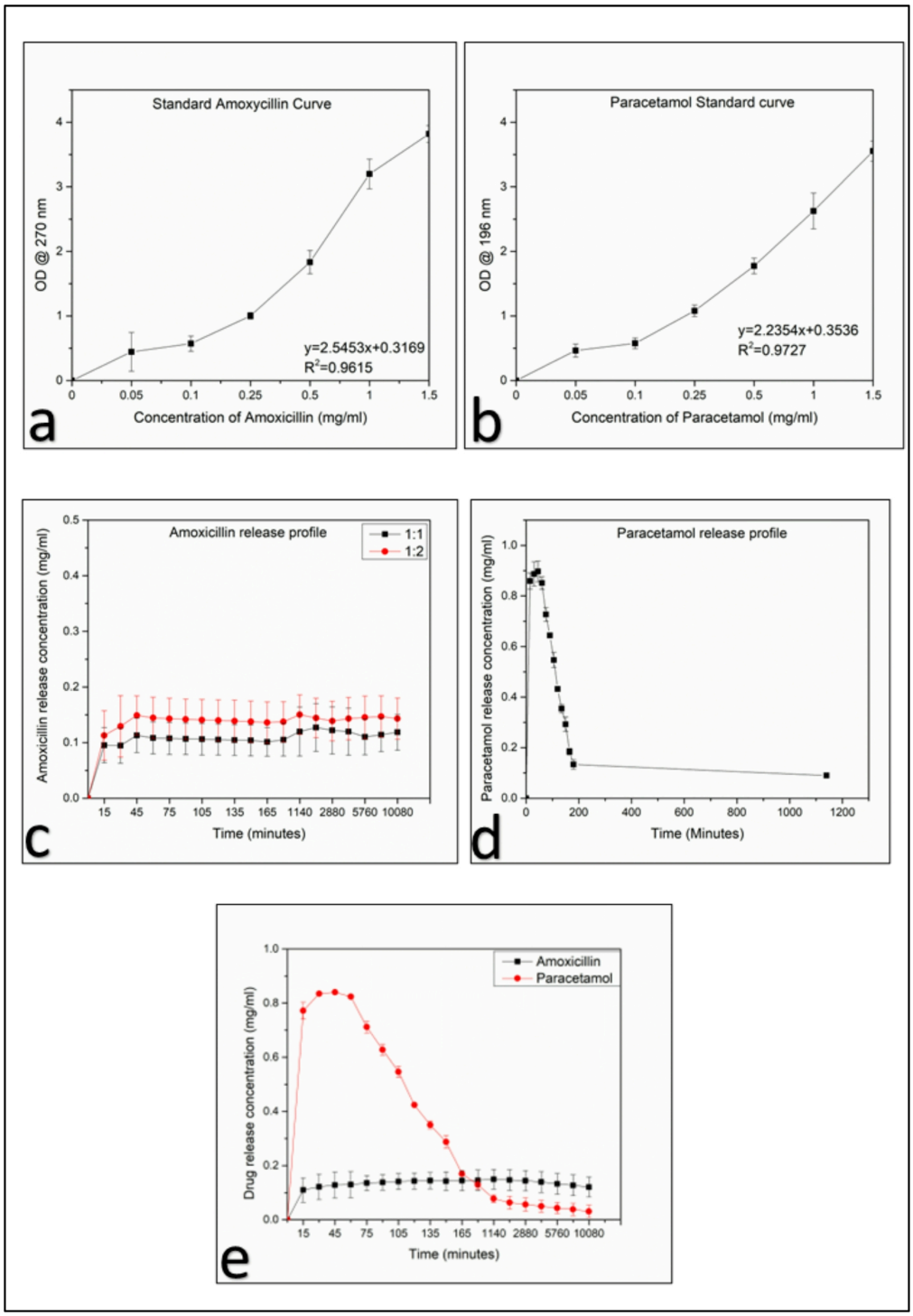


Figure 5

Standard absorption curve for Amoxicillin (a) and Paracetamol(b).Concentration of drug released in PBS (mg/ml)versus time for amoxicillin from 1:1 and 1:2 amoxicillin-capped nHAp scaffolds (c) paracetamol from paracetamol-coated scaffold(d),and paracetamol and amoxicillin from the dual-drug delivery scaffold (e).Data are mean ± SD (n=3).

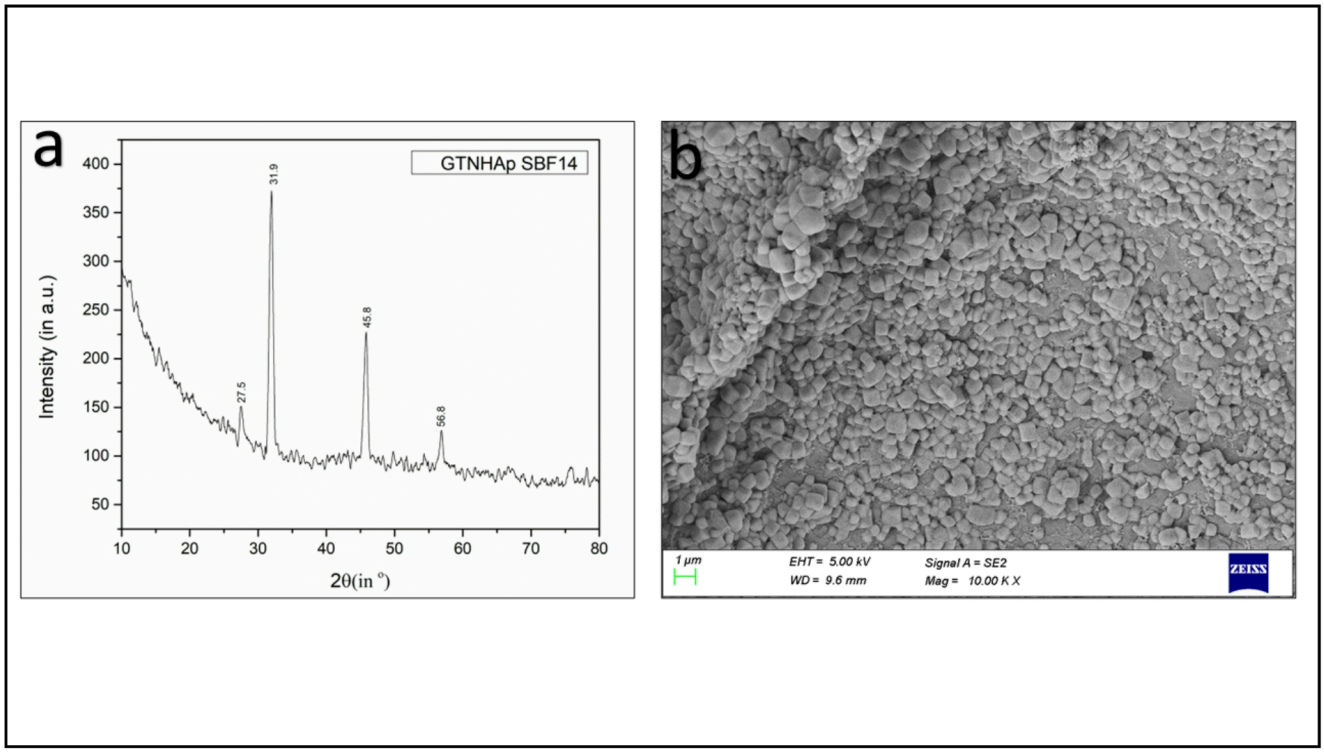


Figure 6

XRD patterns for the scaffold immersed in SBF solution for 14 days show peaks at approximately 2θ=27.5º,31.9º,45.8º and 56.8º corresponding to the (002),(211),(222), and (511) planes of hexagonal hydroxyapatite (JCPDS 09-0432) (a). SEM image of the green tea nHAp integrated alginate scaffold immersed in the SBF solution for 14 days, indicating uniform deposition of hydroxyapatite on the scaffold surface (b).

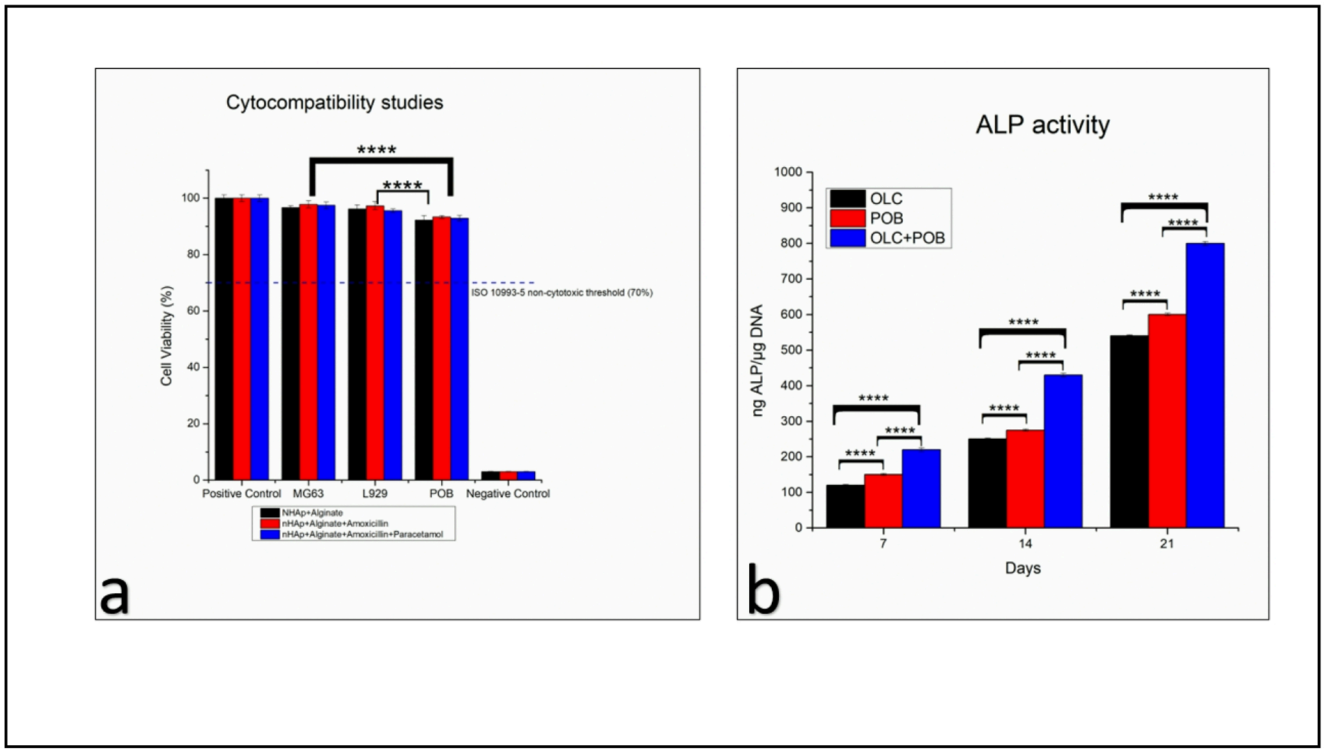


Figure 7

Cytocompatibility studies of nHAp/alginate scaffolds. (a) Cell viability (%) by MTT assay after 48 hours exposure nHAp-alginate scaffolds with drugs (nHAp+alginate+Antibiotic(Amoxicillin),nHAp+Alginate+Antibiotic(Amoxicillin)+Painkiller (Paracetamol))and without the drugs(nHAp+Alginate) against MG63(Human Osteosarcoma cell line),POB (Primary Osteoblasts) and L929 (Mouse fibroblast cell lines).(a); Dashed line : = ISO 10993-5 non-cytotoxic threshold (70%). Negative control=cells treated with cytotoxic agent. ALP activity assay (ng ALP/µg DNA) of nHAp-embedded alginate scaffold against POB(primary osteoblasts) and OLC(Odontoblast-like cells) cell lines at days 7,14, and 21, validating the scaffolds osteogenic property.Positive control=untreated cells, (b). Data are shown as mean ± SD (n = 3). Two-way ANOVA followed by Tukey's HSD post-hoc test. Significance levels: *p < 0.05, **p < 0.01, ***p < 0.001, ****p < 0.0001.

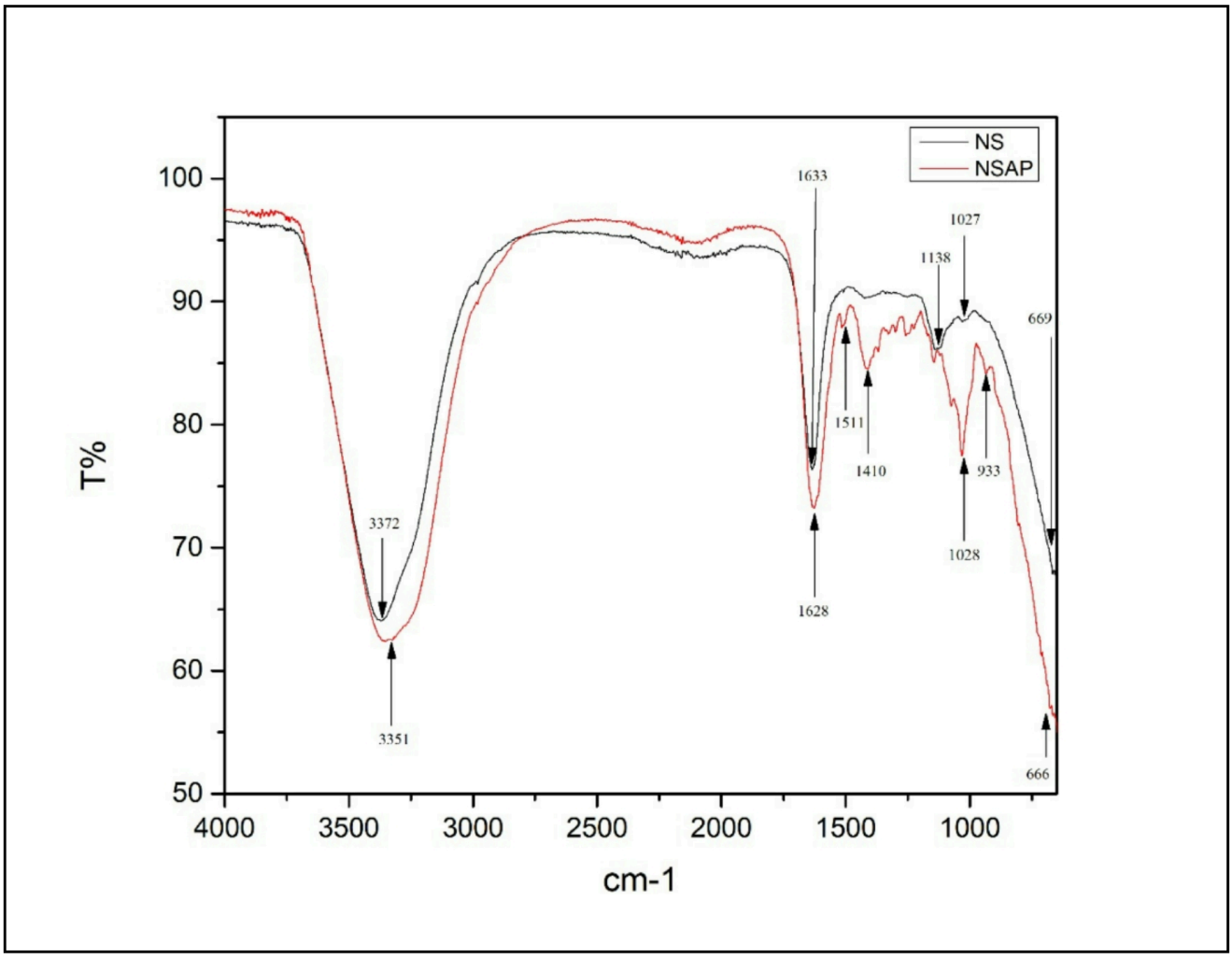


Figure 8

FTIR analysis of nHAp-integrated alginate scaffold (NS) and nHAp-integrated alginate scaffold incorporated with Amoxicillin and Paracetamol (NSAP). The preservation of the characteristic alginate peaks alginate (O–H/carboxylate, ~3372, 1633 cm^{-1}), phosphate (~1027, 669 cm^{-1}) and drug-associated peaks (~1511, 1410 cm^{-1}) without the appearance of new covalent bands indicates that the drugs are held by hydrogen bonding and physical entrapment instead of chemical modification, validating the preservation of the chemical integrity of the scaffold. NS: nHAp-alginate scaffold; NSAP: nHAp -alginate scaffold integrated with amoxicillin and paracetamol.

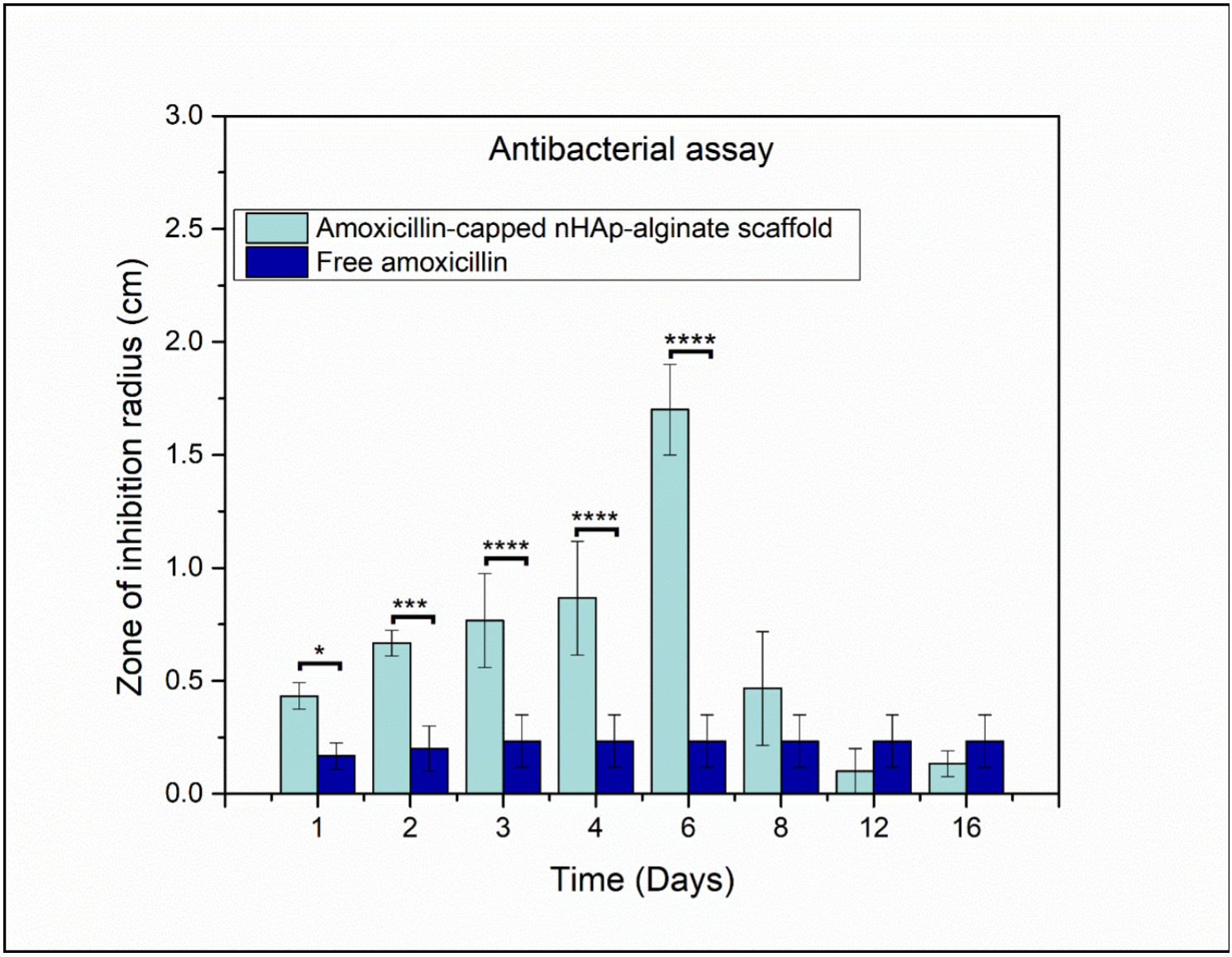


Figure 9

Antibacterial assay carried out on nHAp-alginate scaffold integrated with amoxicillin compared against free amoxicillin. The graph is represented as mean ± SD (n=3). The scaffold integrated with amoxicillin is found to have given a bigger zone of inhibition on day 6 (1.70 ± 0.20 cm), indicating sustained amoxicillin release, in comparison to the free amoxicillin, which gave a burst release and a smaller zone of inhibition (0.23 ± 0.12 cm on day 6). Significance levels: *p < 0.05, **p < 0.01, ***p < 0.001,****p<0.0001;Days 8-16 not significant.